OCEANOGRAPHY

Direct observational evidence of strong CO_2 uptake in the Southern Ocean

Yuanxu Dong[1,2]†*, Dorothee C. E. Bakker[1], Thomas G. Bell[2], Mingxi Yang[2], Peter Landschützer[3], Judith Hauck[4], Christian Rödenbeck[5], Vassilis Kitidis[2], Seth M. Bushinsky[6], Peter S. Liss[1]

The Southern Ocean is the primary region for the uptake of anthropogenic carbon dioxide (CO_2) and is, therefore, crucial for Earth's climate. However, the Southern Ocean CO_2 flux estimates reveal substantial uncertainties and lack direct validation. Using seven independent and directly measured air-sea CO_2 flux datasets, we identify a 25% stronger CO_2 uptake in the Southern Ocean than shipboard dataset–based flux estimates. Accounting for upper ocean temperature gradients and insufficient temporal resolution of flux products can bridge this flux gap. The gas transfer velocity parameterization is not the main reason for the flux disagreement. The profiling float data–based flux products and biogeochemistry models considerably underestimate the observed CO_2 uptake, which may be due to the lack of representation of small-scale high-flux events. Our study suggests that the Southern Ocean may take up more CO_2 than previously recognized, and that temperature corrections should be considered, and a higher resolution is needed in data-based bulk flux estimates.

INTRODUCTION

The Southern Ocean (south of 35°S) is a primary region for anthropogenic carbon dioxide (CO_2) uptake, accounting for ~40% of the total ocean CO_2 sink (*1*, *2*). Yet, it remains the most uncertain region with regard to CO_2 flux estimates (*3*–*5*). This is essentially due to the sparsity of shipboard surface ocean CO_2 fugacity (fCO_{2w}) observations, especially during the austral winter (*6*–*8*). Since 2014, tens of profiling biogeochemical floats have been deployed in the Southern Ocean, and the data collected from these floats have addressed this wintertime data gap (*9*). Flux estimates based on the derived float fCO_{2w} data suggest a considerably weaker Southern Ocean CO_2 sink in all seasons compared to the estimates based on the mainly shipboard dataset (fig. S1) (*10*, *11*). Global ocean biogeochemistry models (GOBMs) also simulate the CO_2 flux (*12*). Although they largely agree with the shipboard fCO_{2w}-based estimates on the annual mean flux (*3*), models have a large spread and indicate a weaker CO_2 sink in austral summer and a stronger CO_2 sink during winter in the Southern Ocean compared to the ship-based estimates (fig. S1).

In addition to uncertainties from sparse fCO_{2w} observations, upper ocean temperature gradients introduce another uncertainty. The fCO_{2w}-based bulk flux estimate is sensitive to the temperature accuracy, and accounting for the ocean cool skin and the warm shipboard temperature bias results in a 15 to 30% increase in the Southern Ocean CO_2 sink (*13*, *14*). The sampling alias (i.e., too-long sampling interval of the data) also leads to uncertainties in the estimate of mean CO_2 flux (*15*, *16*). Intense but small-scale flux events may be important for the mean flux estimate in the Southern Ocean (*17*, *18*). Furthermore, the parameterization of gas transfer velocity (K_{660}) remains a major source of uncertainty in air-sea CO_2 flux estimates (*19*, *20*). Recent eddy covariance (EC) flux observations reveal substantial regional variations in the relationship of K_{660} to wind speed (*21*), but a uniform wind speed–dependent K_{660} is widely used to estimate the CO_2 flux across different ocean regions.

Because of advancements in the EC technique, direct air-sea CO_2 flux measurements on a largely autonomous basis (*22*) are now available to provide an independent constraint on the strength of the Southern Ocean CO_2 sink. The EC technique measures CO_2 flux directly (~10 km^2, hourly resolution), which does not rely on any parameterizations of gas exchange and is thus not subject to subjective and often inconsistent choices of gas transfer velocity. Additionally, this micrometeorology method (i.e., EC) is unaffected by upper ocean temperature gradients and the sampling alias. Therefore, the direct flux measurements by EC provide an independent reference for any air-sea CO_2 flux estimates. Over the period from 2019 to 2020, we collected extensive EC CO_2 flux measurements during seven research cruises in the Southern Ocean (fig. S2). Here, we use these independent flux datasets to assess previous CO_2 flux estimates in the Southern Ocean.

RESULTS

Mean air-sea CO_2 fluxes

We use ~2500 hours (~175 days) of high-quality EC air-sea CO_2 flux measurements (F_{EC}; Fig. 1A) to assess five CO_2 flux estimates (see Materials and Methods) in the summertime (defined as November to April in this study) Southern Ocean:

1) $F_{SOCAT\_corrections}$: flux based on mainly shipboard fCO_{2w} observations in the Surface Ocean CO_2 Atlas (SOCAT) dataset (*6*, *12*) with cool skin and warm bias temperature corrections (*13*)

2) F_{SOCAT}: flux based on SOCAT dataset without cool skin and warm bias corrections

3) F_{SOCCOM}: flux based on profiling float fCO_{2w} estimates from the Southern Ocean Carbon and Climate Observations and Modeling (SOCCOM) program south of 30°S (*9*) and named as SOCCOM-weighted product following a previous study (*10*)

4) $F_{SOCAT+SOCCOM}$: flux based on the combined SOCAT and SOCCOM dataset south of 30°S (*10*)

5) F_{models}: flux from GOBMs (*23*, *24*)

[1]Centre for Ocean and Atmospheric Sciences, School of Environmental Sciences, University of East Anglia, Norwich, UK. [2]Plymouth Marine Laboratory, Plymouth, UK. [3]Flanders Marine Institute (VLIZ), InnovOcean Campus, Ostend, Belgium. [4]Alfred-Wegener-Institut, Helmholtz-Zentrum für Polar- und Meeresforschung, Bremerhaven, Germany. [5]Max Planck Institute for Biogeochemistry, Jena, Germany. [6]School of Ocean and Earth Science and Technology, Department of Oceanography, University of Hawai'i at Mānoa, Honolulu, HI, USA.
*Corresponding author. Email: ydong@geomar.de
†Present address: GEOMAR—Helmholtz Centre for Ocean Research Kiel, Kiel, Germany.

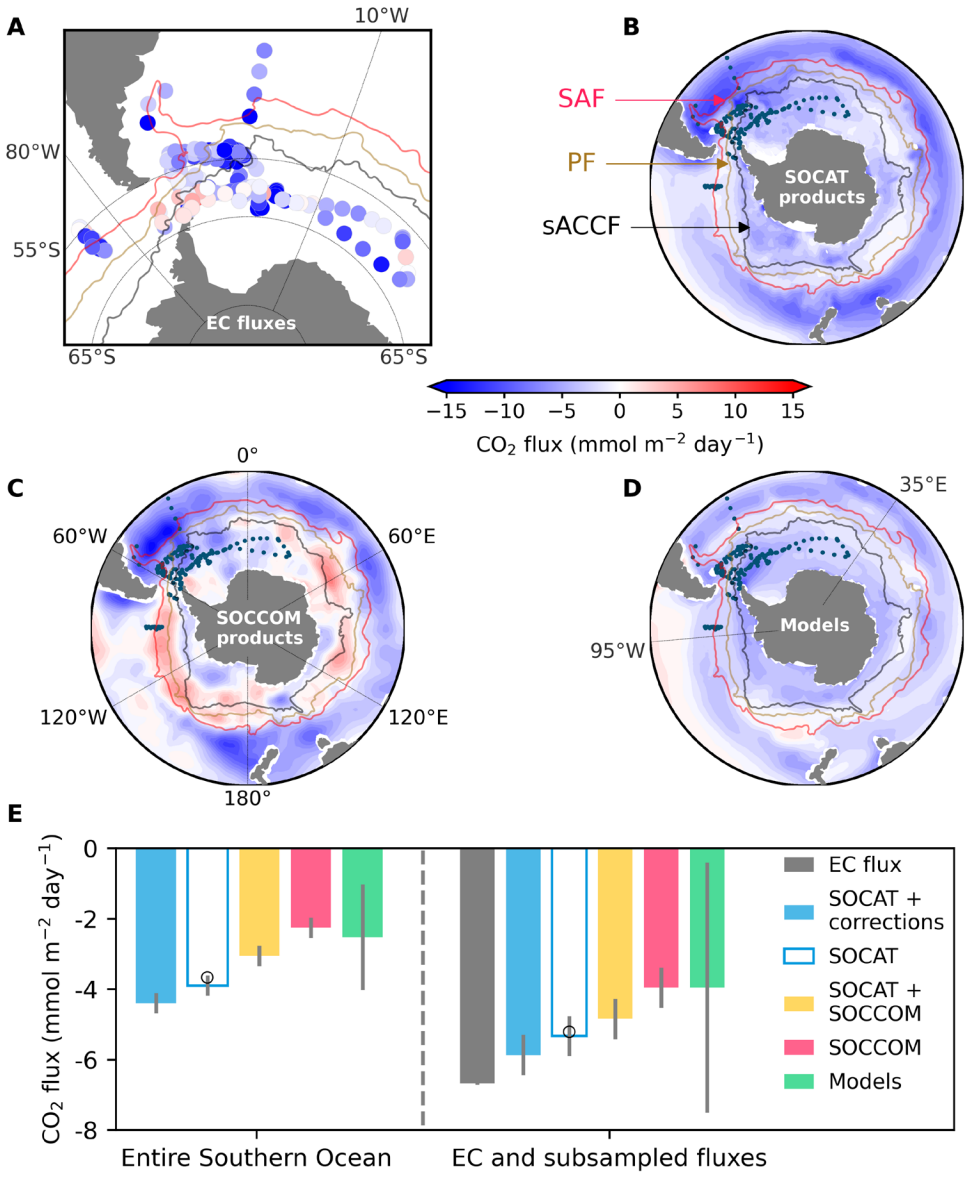

Fig. 1. Austral summer (November to April) air-sea CO_2 flux in the Southern Ocean. (**A**) Daily averaged EC CO_2 flux measurements. Map of shipboard [(**B**), SOCAT]–, float [(**C**), SOCCOM]–, and GOBM [(**D**), models]–based CO_2 flux estimates averaged over 2015 to 2020. (**E**) CO_2 flux estimates for the entire Southern Ocean (left) and the mean of the hourly EC flux and subsampled flux estimates (right). Bars with different colors represent the EC flux measurements (black) and flux estimates from SOCAT-based flux products with (filled blue) and without (unfilled blue) temperature corrections, SOCAT plus SOCCOM–based products (yellow), SOCCOM-weighted products (red), and models (green). The same interpolation methods are used for the filled and unfilled blue bars. Open circles denote the two SOCAT-based flux products yielded through the same available interpolation methods as those for the SOCCOM-weighted products. Error bars indicate one standard deviation (SD) (see Materials and Methods). Fronts constructed from satellite altimetry data (*25*) are shown as red (SAF), brown (PF), and black lines (sACCF). Negative values indicate fluxes into the ocean.

First, F_{SOCCOM} shows prevailing disagreements with F_{SOCAT}, with the former on average 60% lower in magnitude than the latter (Fig. 1E) and their difference is most conspicuous in the frontal zone (Fig. 1, B and C). As expected, $F_{SOCAT+SOCCOM}$ falls between F_{SOCAT} and F_{SOCCOM}. In addition, F_{models} also indicates considerably lower CO_2 uptake than F_{SOCAT}, but their discrepancy is relatively uniform in space (Fig. 1, B and D) and the flux from different models has a large spread, as indicated by the large error bar in Fig. 1E. Furthermore, temperature corrections increase the SOCAT-based CO_2 uptake by 13%. Consequently, our current knowledge of the strength of Southern Ocean CO_2 sink in summer is $F_{SOCAT\_corrections} > F_{SOCAT} > F_{SOCAT+SOCCOM} > F_{SOCCOM} \approx F_{models}$ in magnitude (Fig. 1E).

To assess these flux estimates using our EC data, we subsample the five CO_2 flux products at the time and location of each hourly EC flux measurement. Most of the flux products originally have a 1° by 1°, monthly resolution (see Materials and Methods). The subsampled fluxes are expressed as $F_{SOCAT\_corrections\_sub}$, F_{SOCAT_sub}, F_{SOCCOM_sub}, $F_{SOCAT+SOCCOM\_sub}$, and F_{models_sub}. The EC flux suggests an on average 25% (1.4 mmol m^{-2} day^{-1}) greater CO_2 uptake than F_{SOCAT_sub}, and a smaller (14%) difference with

$F_{SOCAT\_corrections\_sub}$ (Fig. 1E). F_{SOCCOM_sub} and F_{models_sub} (with large uncertainty) indicate a substantially weaker (~70%) CO_2 uptake compared to the EC flux observations. It is worth noting that although the magnitude of the subsampled fluxes exceeds the corresponding mean fluxes for the entire Southern Ocean, the order of the different flux estimates is identical to that for the entire Southern Ocean (Fig. 1E). This suggests that while the observed ocean area is a relatively strong CO_2 uptake region, the order of these five subsampled fluxes can effectively represent that of the entire Southern Ocean.

Regional and temporal breakdown

The disagreement of the Southern Ocean CO_2 flux among different estimates is not uniform in both space and time (Fig. 1 and fig. S1). Our extensive EC dataset, collected over 6 months during seven cruises and covering vast regions, allows for a comprehensive comparison with flux estimates across different regions and months. Notably, the SOCAT plus SOCCOM–based flux consistently falls between the SOCAT-based and SOCCOM-weighted flux estimates (fig. S1), and thus is excluded for the subsequent comparisons.

Previous research emphasizes the critical role of oceanographic fronts in driving discrepancies in different CO_2 flux estimates (*10*, *11*). Here, we categorize the observed EC and subsampled fluxes into four distinct regions (*25*): between 35°S and the Subantarctic Front (SAF), between SAF and the Polar Front (PF), between PF and the southern Antarctic Circumpolar Current (sACCF), and south of sACCF (Fig. 1). Across all four regions, the EC flux shows consistently stronger CO_2 uptake compared to all the subsampled flux estimates (Fig. 2A). The discrepancy value between F_{EC} and F_{SOCAT_sub} is relatively constant, and when accounting for the temperature corrections, the SOCAT-based flux estimate agrees better with the EC flux. F_{SOCCOM_sub} is substantially lower in magnitude than F_{EC}, especially south of sACCF and in the area between SAF and PF. F_{EC} suggests a CO_2 uptake approximately 2.5 times greater than F_{SOCCOM_sub} south of sACCF, while $F_{SOCAT\_corrections\_sub}$ is very similar to the EC flux in this region. Given that most of our observations were south of the sACCF, the comparison in this region should be relatively robust. On a bimonthly timescale, the independent EC flux agrees reasonably well with $F_{SOCAT\_corrections\_sub}$, while F_{EC} suggests consistently greater CO_2 uptake compared to other subsampled flux estimates (Fig. 2B). F_{SOCCOM_sub} substantially underestimates the observed EC flux, particularly in March and April.

In summary, the reasonable agreement between the EC flux and $F_{SOCAT\_corrections\_sub}$, alongside the substantial discrepancy between the EC flux and F_{SOCCOM_sub} as shown in Fig. 1E, aligns coherently with the regional and temporal breakdown (see also the latitudinal and longitudinal breakdown in fig. S3). Moreover, the difference between F_{SOCAT_sub} and F_{EC} is relatively consistent, while the discrepancy between F_{SOCCOM_sub} and F_{EC} is not uniform.

Small-scale flux variability

The typical resolution of most CO_2 flux products is 1° by 1° and monthly. The EC air-sea CO_2 flux has a much higher temporal resolution of 1 hour and spatial resolution spanning ~10 km^2. These high-frequency EC flux data provide valuable insights into small-scale flux variability. To reduce the random uncertainty, the hourly EC fluxes (fig. S4) are presented as a daily running mean in Fig. 3A (see Materials and Methods). The EC flux reveals mostly periods of

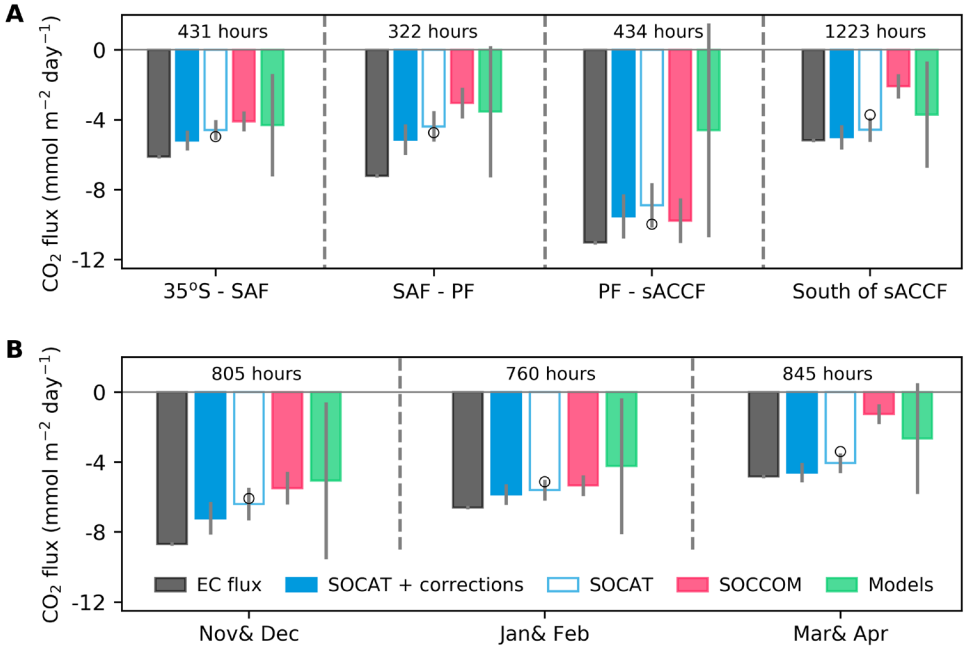

Fig. 2. Regional and temporal breakdown of the EC CO_2 flux measurements and subsampled flux estimates. In (**A** and **B**), the five bars with different colors represent the hourly EC flux measurements from the seven cruises (black), subsampled flux from SOCAT-based flux products with (filled blue) and without (unfilled blue) temperature corrections, SOCCOM-based flux products (red), and models. Open circles denote the two SOCAT-based flux products obtained using the same available interpolation methods as those for the SOCCOM-weighted products. Error bars reflecting one SD provide a measure of uncertainty (see Materials and Methods). Refer to the caption of Fig. 1 for the definition of the fronts SAF, PF, and sACCF. The number of hours of matched EC flux and subsampled flux is indicated above each subplot.

ocean CO_2 uptake with occasional short-lived outgassing events (Fig. 3A). The subsampled SOCAT-based and SOCCOM-weighted flux products closely track the daily EC flux variations (Fig. 3A) with a moderately to highly positive correlation coefficient (0.73 and 0.55, respectively). This suggests that the flux products based on the sparse fCO_{2w} data can reproduce the small-scale flux variability rather well. In addition, F_{SOCCOM_sub} indicates sustained CO_2 outgassing during cruise JR18005 and a near-neutral flux environment during cruise DY111. Conversely, the direct EC flux observations suggest predominantly CO_2 uptake during both cruises, supporting the SOCAT-based flux estimate. While the subsampled model flux can reflect the background flux signal, it does not capture most of

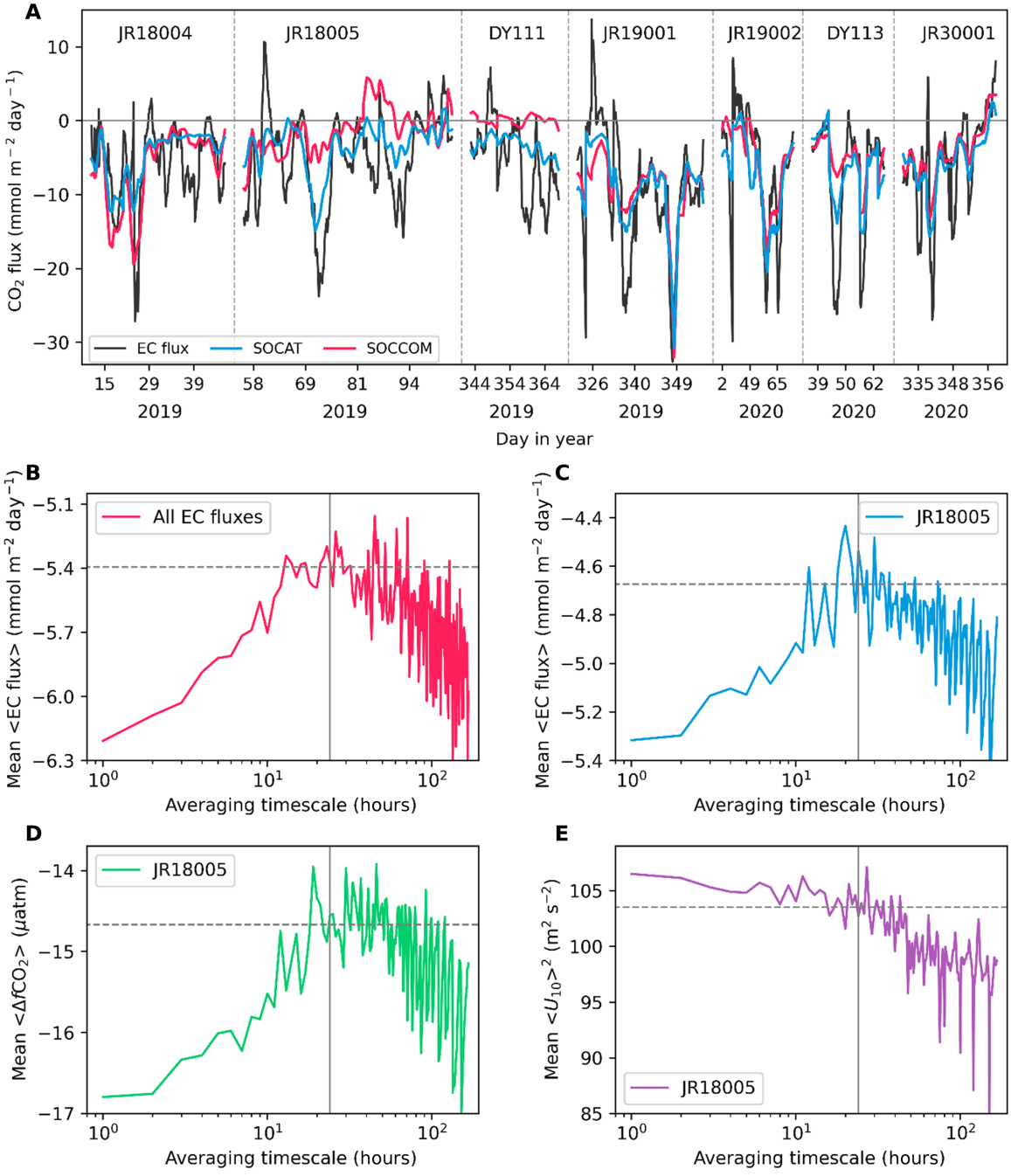

Fig. 3. Flux time series with a daily running mean and the mean of the variables with different averaging timescales. (**A**) EC air-sea CO_2 flux measurements from seven Southern Ocean cruises (black) and subsampled flux estimates from the average of two SOCAT-based flux products (blue) and two SOCCOM-weighted flux products (red) at the time and location of each hourly EC measurement, respectively. Note that fCO_{2w} observations from four (JR18004, JR18005, JR19001, and JR19002) of our seven cruises have been included in the SOCAT v2021 dataset. (**B**) Mean of the entire EC flux from seven cruises with different averaging timescales. (**C** to **E**) Mean of the EC flux (C), air-sea CO_2 fugacity difference from the ship's underway equilibrator fCO_2 system [ΔfCO_2, (D)], and the square of 10-m wind speed [U_{10}, (E)] from cruise JR18005 with different averaging timescales. Note that all data in (C) to (E) are independent measurements. The solid-vertical line represents the 1-day timescale, and the dashed-horizontal line denotes the average of the mean flux with timescales between 16 and 32 hours.

the daily EC flux variations ($r = 0.05$; fig. S5), which is unsurprising because models have not been inherently designed to simulate small-scale flux processes.

None of the flux estimates can well capture the short-lived, high-flux events, which is potentially due to the coarse resolution of these flux products. However, these high-flux events may be important for the large-scale mean flux estimates. One of the SOCAT-based products [CarboScope, (*26*)] originally has a daily resolution. The subsampled daily CarboScope flux captures more high-flux events than the subsampled monthly aggregated flux (fig. S6), and the mean of the former is 13% higher in magnitude than the latter. Figure 3B suggests that the mean of the EC flux is sensitive to the averaging timescale with a ~15% flux decrease in magnitude from an hourly to a half-day scale. The mean EC flux has no obvious trend from a half day to 2 days, suggesting the steady state of the mean flux at this timescale domain. Beyond 2 days, the mean CO_2 uptake shows an increasing trend with large fluctuations, which may be because the research vessels move across large regions and the natural spatial heterogeneity compromises the timescale sensitivity. This is supported by evidence that the mean of the subsampled monthly SOCAT-based flux products (i.e., F_{SOCAT_sub}) is expected to have no trends, but shows an increasing trend in magnitude at timescales higher than 2 days (fig. S7). Thus, we do not consider the EC flux timescale analysis beyond 2-day timescales. The 15% EC flux decrease in magnitude from the hourly to the daily timescale can bridge the gap between F_{EC} and $F_{SOCAT\_corrections\_sub}$ (14%). We use the observations from cruise JR18005, which has the fewest data gaps compared to other cruises (fig. S4), to test the possible reason for the mean flux sensitivity to the averaging timescale. The mean EC flux from JR18005 also shows a typical ~15% decrease in magnitude from an hourly to a half-day scale (Fig. 3C), which is primarily due to the decrease in the magnitude of ΔfCO_2 instead of the wind speed (Fig. 3, D and E). This averaging timescale effect is essentially the sampling alias (i.e., sampling at insufficient spatial-temporal resolution). The change of the mean EC flux with the sampling interval (fig. S8) is similar to the change of the mean EC flux with the averaging timescale (Fig. 3).

Gas transfer velocity

The gas transfer velocity (K_{660}) is a key parameter in both the fCO_{2w}-based and model-based air-sea CO_2 flux estimates (see Materials and Methods) and is often a source of inconsistency between estimates. Studies show that the uncertainty in the K_{660} parameterization dominates the overall uncertainty in global ocean CO_2 uptake estimates [e.g., (*19*, *20*, *27*)]; thus, it behooves us well to test whether the discrepancies observed above can be linked to differences in the gas transfer. A common wind speed–dependent K_{660} constrained by the global bomb-^{14}C inventory (K_{660_14C}) (*19*) is used for CO_2 flux estimates for the global ocean (*12*). However, a recent study shows that the K_{660}–wind speed relationship has substantial regional variations, especially at low and high wind speeds (*21*). Our EC air-sea CO_2 flux observations coupled with simultaneous fCO_{2w} observations made during the same cruise provide an opportunity to constrain K_{660} for the Southern Ocean environment from low to high wind speeds (see Materials and Methods). To minimize the impact of the cool skin effect on the EC-derived K_{660}, we only use the data with $|\Delta fCO_2| > 40$ μatm for the parametrization. A total of 553 hours of K_{660} values are derived after quality control (Fig. 4), which is so far the most extensive ship-based high-quality K_{660} dataset in the Southern Ocean with consistent experimental setup and data processing (*22*).

The EC-derived K_{660} (K_{660_EC}) on average agrees well with the K_{660_14C} at intermediate wind speeds (Fig. 4). However, K_{660_EC} is higher at low wind speeds and lower at high wind speeds compared to K_{660_14C}, which is likely related to chemical enhancement and ocean waves (see Supplementary Text). Although this divergence is small (1 to 2 cm hour^{-1}), it is notable in comparison to the global mean of gas transfer velocity (16.5 cm hour^{-1}) (*28*). The results presented in Fig. 4 are based on the in situ wind speed measurements during our Southern Ocean cruises, while the fCO_{2w}-based flux estimates typically rely on a reanalysis wind speed product (e.g., ERA5 and JRA55; see Materials and Methods). The mean difference between the square of the subsampled reanalysis wind speed product and the in situ wind speed is small (~3%). The use of subsampled wind speed from different wind products to parameterize K_{660} introduces slight changes in the coefficient (fig. S9). Nevertheless, the EC-based K_{660} consistently remains higher at low wind speeds and lower at high wind speeds compared to the ^{14}C-based K_{660} parameterization (fig. S9). The re-calculation of F_{SOCAT_sub} using either our EC-based or the ^{14}C-based K_{660}–wind speed parameterization does not yield a substantial difference in the mean flux (~5%) and thus cannot explain the large difference in flux observed in Figs. 1 and 2. This is because intermediate wind speed (5 to 13 m s^{-1}) conditions dominate our observations (Fig. 4), while the enhanced CO_2 uptake at low wind speeds largely counteracts the dampened uptake at high wind speeds.

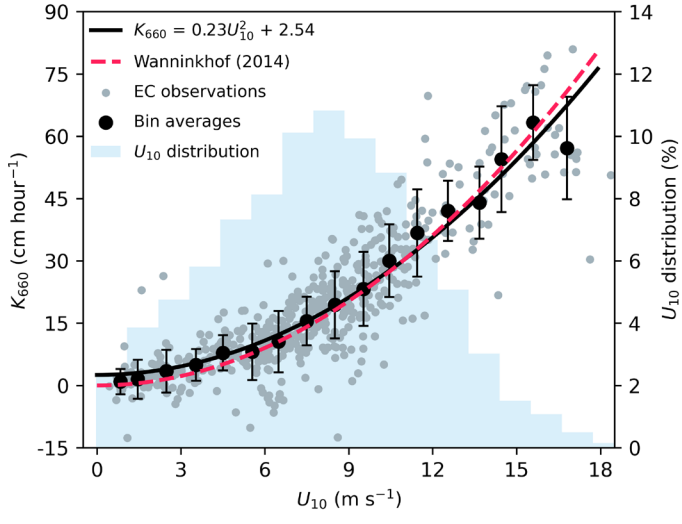

Fig. 4. Gas transfer velocities (K_{660}) derived from EC air-sea CO_2 flux observations. Gray dots are hourly EC-derived K_{660} (553 hours), and black circles represent 1 m s^{-1} bin averages, with error bars indicating one SD. The black curve represents the least square fit using the bin averages ($R^2 = 0.78$). The red dashed line corresponds to a K_{660} parameterization based on the global ^{14}C inventory (*19*). Negative K_{660} values are due to uncertainties in EC fluxes and fCO_2 observations. Light blue bars denote the frequency distribution of in situ wind speeds (U_{10}) during our cruises.

DISCUSSION

The independent EC air-sea CO_2 flux measurements suggest greater CO_2 uptake than the subsampled SOCAT-based flux estimates (Figs. 1E and 2). The EC flux agrees better with the temperature-corrected SOCAT-based flux estimates (*13*). A previous study (*14*) reported a theoretically ~30% (0.35 Pg C year^{-1}) increase in the SOCAT-based CO_2 uptake in the Southern Ocean by considering the temperature effects (i.e., the ocean cool skin effect and the potential warm bias induced by the ship's engine heating). This figure is revised to ~15% (0.2 Pg C year^{-1}) with an updated assessment of these two temperature effects (*13*). This study provides observational evidence emphasizing the need to take these two temperature effects into account in SOCAT-based bulk flux estimates. Additionally, recent aircraft measurements in the south of 45°S also indicate a stronger ocean CO_2 sink signal compared to F_{SOCAT}, in agreement with this study (fig. S10) (*29*). Furthermore, the uncorrected SOCAT-based air-sea CO_2 flux products (*12*), incorporating a riverine flux adjustment (*30*), yield a cumulative anthropogenic CO_2 uptake of 47.9 Pg C for the decades 1994 to 2014. This is smaller than the anthropogenic CO_2 uptake of 56.6 Pg C indicated by the interior ocean carbon inventory over the same period (*31*). The temperature corrections (*13*) increase the SOCAT-based CO_2 uptake by 11.2 Pg C, bridging the gap between SOCAT-based and interior ocean inventory–based CO_2 sink estimates, and resulting in near-zero non–steady-state natural carbon flux over these two decades. It is worth noting that the argument for considering the temperature corrections is from the comparison between F_{EC} and F_{SOCAT}, but stronger evidence should be based on direct comparisons between F_{EC} and the bulk flux calculated by the simultaneously measured fCO_2. However, our data collected by the research vessel is frequently calibrated and thus is free from the warm bias issue, and the impact of the cool skin correction on the in situ bulk flux is relatively small (−0.13 mmol m^{-2} day^{-1}) compared to the large background flux in the regions with fCO_2 observations (−5.5 mmol m^{-2} day^{-1}). The in situ bulk flux shows good agreement with the EC flux (fig. S4B). A large fraction of the SOCAT data was collected by volunteer ships and lacked temperature calibration. Thus, both the warm bias and the cool skin effect have impacts on F_{SOCAT}. Dedicated experiments with simultaneous EC and fCO_2 observations at regions with $|\Delta fCO_2|$ close to zero will be required to further confirm the cool skin flux correction.

The remaining difference between F_{EC} and $F_{SOCAT\_corrections\_sub}$ can be explained by the insufficient temporal resolution of the SOCAT-based flux products (sampling alias). The high-flux events lasting less than a day are important for the mean flux estimate. Averaging over a too-long timescale or sampling over a too-large interval will dampen this high-flux effect and result in an underestimate of the mean CO_2 flux (Fig. 3B). This sampling effect is mainly driven by the ΔfCO_2 in our datasets (Fig. 3D), suggesting the need for high-resolution ΔfCO_2 observations (i.e., hourly) and reconstruction in the Southern Ocean [fig. S6; (*15*–*18*)].

Relative to our independent EC flux data, the subsampled SOCCOM-weighted flux substantially underestimates the ocean CO_2 uptake (Fig. 2). Particularly, a continuous CO_2 outgassing period indicated by F_{SOCCOM_sub} is not supported by the EC flux observations, which suggest CO_2 uptake (Fig. 3). The CO_2 outgassing signal from F_{SOCCOM} is also not corroborated by the Southern Ocean aircraft campaigns (*29*). Moreover, the disagreement between F_{SOCCOM} and F_{SOCAT} not only is evident in winter but also prevails in summer (Fig. 1), the season when SOCAT contains more fCO_{2w} data than SOCCOM (fig. S11). Therefore, the disagreement between F_{SOCCOM} and F_{SOCAT} cannot be simply attributed to the sparsity in fCO_{2w} observations. Possible explanations for the mismatch include that SOCCOM fCO_{2w} values are not direct measurements but are derived from pH observations and total alkalinity estimates (*32*). Thus, the SOCCOM fCO_{2w} estimates have much larger theoretical uncertainties (±11 μatm) (*32*) compared to those of shipboard fCO_{2w} measurements (±2 to 5 μatm) (*6*). A positive bias may exist in these float fCO_{2w} estimates (+2 to +6 μatm) (*11*, *32*–*35*). It is also possible that fCO_{2w} mapping methods extrapolate local biased signals to the wider Southern Ocean. Correcting for an on average +4 μatm bias reduces the mean flux difference between F_{SOCCOM_sub} and F_{EC} already by half. Furthermore, the sampling alias may also be partially responsible for the underestimation of the SOCCOM-weighted flux given that the SOCCOM floats operate at a ~10-day sampling frequency (*9*). A recent study found that subsampling an hourly flux dataset in the Southern Ocean with a 10-day frequency results in a 23% positive bias (more outgassing/less uptake) in the mean flux (*16*). Another study indicates ±50% uncertainty in the mean flux with a 10-day sampling period, while the uncertainty is only 5% at a daily sampling frequency (*15*). Thus, we advocate against the use of the SOCCOM-weighted flux reconstruction, which was intended as an idealized experiment (*10*).

The ensemble mean of the eight process models considerably underestimates the observed EC air-sea CO_2 flux (Figs. 1 and 2), and the subsampled fluxes from eight individual models have a large spread and different agreement with the EC flux (fig. S12). This is likely due to the models' inadequate representation of biological processes in the summertime Southern Ocean (*3*) and insufficient resolution for capturing the small-scale processes (*17*). Notably, fCO_2 observation–based CO_2 flux estimates suggest a relatively robust capacity to reproduce daily flux variabilities (Fig. 3), which may provide valuable insights for refining models.

The gas transfer velocities derived from our EC CO_2 flux measurements provide a constraint for K_{660} from low to high wind speeds at a scale (several square kilometers, hourly) comparable to that of the gas exchange processes. The good agreement in the bulk fluxes between using our EC-based K_{660} and the global ^{14}C-based K_{660} (*19*) implies that the flux discrepancies presented in this study are not mainly due to K_{660}. Consequently, the primary challenge in the Southern Ocean CO_2 flux estimate lies in fCO_2, highlighting the critical importance of sustaining efforts in high-quality and high-resolution fCO_{2w} observations. However, this fCO_{2w} collection effort has drastically declined in recent years and the number of the annual datasets in SOCAT decreased by 35% from 2017 to 2021 (40% in the Southern Ocean) (*36*).

This study suggests that the Southern Ocean may absorb more CO_2 than previously recognized. It provides observational evidence for applying the temperature corrections and considering the sufficient temporal resolution in the shipboard dataset–based bulk flux estimates. In addition, the float-based flux product and models substantially underestimate the observed CO_2 uptake. Noting that our cruise data only cover some part of the Southern Ocean in summer, continued efforts toward high-quality EC flux and fCO_{2w} observations are essential to improve the estimate of air-sea CO_2 fluxes. This may include an expansion of simultaneous EC flux and fCO_{2w} measurements to more ships, and possibly the further deployment of buoys and Sail drones, especially for measurements in low $|\Delta fCO_2|$

region to test the cool skin effect and the winter season with high speed. Moreover, refined resolutions in the fCO_{2w} reconstruction and model simulation should be a focus of future work.

MATERIALS AND METHODS

Direct flux measurements by EC

EC fluxes are measured in the atmosphere and do not rely on fCO_2 measurements and gas transfer velocity parameterization. The air-sea CO_2 flux F is measured directly by the EC technique and is calculated using

$$F = \rho\overline{w'c'} \quad (1)$$

where ρ is the mean mole density of dry air (e.g., in mol m^{-3}). The CO_2 mixing ratio in dry air c [in parts per million (ppm) or μmol mol^{-1}] is measured by a fast-response gas analyzer with a dryer, and the vertical wind velocity w (in m s^{-1}) is measured by a sonic anemometer and corrected for the ship's motion. The prime denotes the fluctuations from the mean, while the overbar indicates the time average during the flux calculation interval: 20 min in this study. The sign of the EC flux is determined by the net number of CO_2 molecules invading into and evading from the surface ocean within a flux interval.

Seven research cruises (fig. S2) were conducted in the Southern Ocean on two UK ships in the austral summer of 2019 and 2020. Air-sea CO_2 fluxes were measured using a state-of-the-art closed-path EC system (Picarro G2311-f on RRS *James Clark Ross*, LI-7200 on RRS *Discovery*) with a dryer to eliminate the impact of water vapor fluctuations on the CO_2 flux measurements during all these cruises (*22*). The EC data have been processed and filtered to meet the stationarity requirement of the EC method (*22*). EC flux measurements in regions with sea ice and close to land (distance from land less than 30 km) were removed to avoid confounding the open ocean. In total, we obtained ~3300 hours of quality-controlled EC air-sea CO_2 flux measurements, corresponding to 175 days (at least 4 hours required per day to ensure the representativeness), which is so far the largest ship-based EC CO_2 flux dataset with consistent instrumental setup and data processing. The random uncertainty in the hourly EC flux (~2 mmol m^{-2} day^{-1}) will be considerably reduced after averaging over n hours ($2/\sqrt{n}$) (*22*). Detailed descriptions of these cruises and the EC system are given in the Supplementary Materials.

Bulk air-sea CO_2 flux and product subsampling

Air-sea CO_2 flux can be indirectly estimated by the bulk equation

$$F = K_{660}(Sc/660)^{-0.5}\,(\alpha_{ss}fCO_{2w} - \alpha_s fCO_{2a}) \quad (2)$$

where K_{660} (cm $hour^{-1}$) is the normalized gas transfer velocity at a Schmidt number (Sc) of 660 (*37*). α_{ss} and α_s are the CO_2 solubility (mol $liter^{-1}$ atm^{-1}) (*38*) in the subskin and skin layers in seawater, respectively (*39*). fCO_{2a} (fCO_{2w}) is the atmospheric (seawater) CO_2 fugacity (in μatm). The current fCO_{2w}-based flux products generally neglect the cool skin correction by assuming that α_{ss} is equal to α_s and using the same seawater temperature to calculate both.

To estimate the global ocean CO_2 flux with Eq. 2, interpolating the sparse fCO_{2w} measurements to the global ocean is a key step. Seven SOCAT (*6*) v2021 dataset–based fCO_{2w} products using seven interpolation methods (*26*, *40*–*45*) have been made available for the Global Carbon Budget 2021 (GCB2021) (*23*). Among the seven interpolation methods, two of them [MPI-SOMFFN (*44*) and CarboScope (*26*)] have also been used to interpolate the SOCCOM fCO_{2w} estimates and the SOCAT plus SOCCOM datasets in the Southern Ocean from 2015 to 2020 inclusive (*10*). The fCO_{2w} product is combined with a global wind speed product [e.g., ERA5, (*46*)], a sea surface temperature [e.g., OISST v2, (*47*)] and salinity product, and a global fCO_{2a} product (NOAA Marine Boundary Layer dry air mixing ratio of atmospheric CO_2 and corrected for water vapor pressure) to generate the CO_2 flux product. We subsample CO_2 fluxes from the seven SOCAT-based flux products (F_{SOCAT_sub}) according to the time and location of the hourly EC observations. Then, we subsample the cool skin effect and warm bias flux corrections at a 1° by 1°, monthly resolution (*13*) and apply these flux corrections to F_{SOCAT_sub} to produce the temperature-corrected CO_2 flux subsamples ($F_{SOCAT\_corrections\_sub}$). The cool skin effect is simulated by a physical model (*48*), while the warm temperature bias is assessed by the buoy temperature dataset (*49*). The two SOCCOM-weighted (F_{SOCCOM_sub}) and two SOCAT plus SOCCOM–based ($F_{SOCAT+SOCCOM\_sub}$) flux products are also subsampled at the time and location of the hourly EC observations. See Supplementary Text for how the SOCCOM data are being used in the interpolation process. The products are subsampled from their original resolutions (i.e., 2° latitude by 2.5° longitude, daily for CarboScope; 1° by 1°, monthly for the remaining products). The ensemble mean of the corresponding dataset-based flux products is used for analysis, and the SD of these seven individual SOCAT-based flux products is considered as the uncertainty for $F_{SOCAT\_corrections\_sub}$, F_{SOCAT_sub}, F_{SOCCOM_sub}, and $F_{SOCAT+SOCCOM\_sub}$. The impact of the product resolution on the flux comparison is shown in fig. S6. Note that some of the fCO_{2w} data from our Southern Ocean cruises have been included in the SOCAT v2021 dataset (see Supplementary Text). In total, ~2500 hours of EC flux are matched with all the subsampled flux estimates and these matched data are used for comparison.

GOBMs constrain the air-sea CO_2 flux by the transport of dissolved inorganic carbon from the surface into the ocean interior (*24*). We resampled CO_2 flux from eight models (1° by 1°, monthly) used in GCB2021 (*23*) according to the time and location of the hourly EC observations. The ensemble mean of these eight subsampled model fluxes (F_{models_sub}) is used for analysis, and their SD is assigned as the model flux uncertainty. Note that the model flux represents the anthropogenic CO_2 sink, and the riverine flux should be adjusted to make it comparable with the EC flux observations and the fCO_{2w}-based flux estimates. Nevertheless, the riverine flux in the Southern Ocean, although highly uncertain, is small according to a recent study (*50*) and is thus neglected in this study following the REgional Carbon Cycle Assessment and Processes Project Phase 2 (*3*).

Gas transfer velocity derived from EC fluxes

Gas transfer velocities are derived from hourly EC CO_2 flux observations combined with hourly air-sea CO_2 fugacity measurements

$$K_{660} = \rho\overline{w'c'} / [(\alpha_{ss}fCO_{2w} - \alpha_s fCO_{2a})(Sc/660)^{-0.5}] \quad (3)$$

fCO_{2w} and fCO_{2a} were measured with a showerhead equilibrator attached to the ship's underway system (*51*) during the seven cruises in the Southern Ocean. In total, ~2500 hours of fCO_2 were collected, with approximately half containing both quality-controlled EC CO_2 flux and fCO_2 observations. To reduce the relative uncertainty in the EC air-sea CO_2 flux, minimize the relative impact of the cool skin effect, and enable an optimal analysis, the derived K_{660} was filtered to exclude periods when $|fCO_{2w} - fCO_{2a}|$ was less than 40 μatm.

Supplementary Materials

This PDF file includes:

Supplementary Text
Figs. S1 to S12
Table S1
References

REFERENCES AND NOTES

1. S. Khatiwala, F. Primeau, T. Hall, Reconstruction of the history of anthropogenic CO_2 concentrations in the ocean. *Nature* **462**, 346–349 (2009).
2. N. Gruber, P. Landschützer, N. S. Lovenduski, The variable Southern Ocean carbon sink. *Annu. Rev. Mar. Sci.* **11**, 159–186 (2019).
3. J. Hauck, L. Gregor, C. Nissen, L. Patara, M. Hague, P. Mongwe, S. Bushinsky, S. C. Doney, N. Gruber, C. Le Quéré, M. Manizza, M. Mazloff, P. M. S. Monteiro, J. Terhaar, The Southern Ocean carbon cycle 1985–2018: Mean, seasonal cycle, trends, and storage. *Global Biogeochem. Cycles* **37**, e2023GB007848 (2023).
4. T. DeVries, C. Le Quéré, O. Andrews, S. Berthet, J. Hauck, T. Ilyina, P. Landschützer, A. Lenton, I. D. Lima, M. Nowicki, J. Schwinger, R. Séférian, Decadal trends in the ocean carbon sink. *Proc. Natl. Acad. Sci. U.S.A.* **116**, 11646–11651 (2019).
5. P. Rustogi, P. Landschützer, S. Brune, J. Baehr, The impact of seasonality on the annual air-sea carbon flux and its interannual variability. *npj Clim. Atmos. Sci.* **6**, 66 (2023).
6. D. C. E. Bakker, B. Pfeil, C. S. Landa, N. Metzl, K. M. O'Brien, A. Olsen, K. Smith, C. Cosca, S. Harasawa, S. D. Jones, S. Nakaoka, Y. Nojiri, U. Schuster, T. Steinhoff, C. Sweeney, T. Takahashi, B. Tilbrook, C. Wada, R. Wanninkhof, S. R. Alin, C. F. Balestrini, L. Barbero, N. R. Bates, A. A. Bianchi, F. Bonou, J. Boutin, Y. Bozec, E. F. Burger, W.-J. Cai, R. D. Castle, L. Chen, M. Chierici, K. Currie, W. Evans, C. Featherstone, R. A. Feely, A. Fransson, C. Goyet, N. Greenwood, L. Gregor, S. Hankin, N. J. Hardman-Mountford, J. Harlay, J. Hauck, M. Hoppema, M. P. Humphreys, C. W. Hunt, B. Huss, J. S. P. Ibánhez, T. Johannessen, R. Keeling, V. Kitidis, A. Körtzinger, A. Kozyr, E. Krasakopoulou, A. Kuwata, P. Landschützer, S. K. Lauvset, N. Lefèvre, C. Lo Monaco, A. Manke, J. T. Mathis, L. Merlivat, F. J. Millero, P. M. S. Monteiro, D. R. Munro, A. Murata, T. Newberger, A. M. Omar, T. Ono, K. Paterson, D. Pearce, D. Pierrot, L. L. Robbins, S. Saito, J. Salisbury, R. Schlitzer, B. Schneider, R. Schweitzer, R. Sieger, I. Skjelvan, K. F. Sullivan, S. C. Sutherland, A. J. Sutton, K. Tadokoro, M. Telszewski, M. Tuma, S. M. A. C. van Heuven, D. Vandemark, B. Ward, A. J. Watson, S. Xu, A multi-decade record of high-quality fCO2 data in version 3 of the Surface Ocean CO2 Atlas (SOCAT). *Earth Syst. Sci. Data* **8**, 383–413 (2016).
7. L. Gloege, G. A. McKinley, P. Landschützer, A. R. Fay, T. L. Frölicher, J. C. Fyfe, T. Ilyina, S. Jones, N. S. Lovenduski, K. B. Rodgers, S. Schlunegger, Y. Takano, Quantifying errors in observationally based estimates of ocean carbon sink variability. *Global Biogeochem. Cycles* **35**, 1–14 (2021).
8. J. Hauck, C. Nissen, P. Landschützer, C. Rödenbeck, S. Bushinsky, A. Olsen, Sparse observations induce large biases in estimates of the global ocean CO_2 sink: An ocean model subsampling experiment. *Philos. Trans. R. Soc. A Math. Phys. Eng. Sci.* **381**, 20220063 (2023).
9. L. D. Talley, I. Rosso, I. Kamenkovich, M. R. Mazloff, J. Wang, E. Boss, A. R. Gray, K. S. Johnson, R. M. Key, S. C. Riser, Southern Ocean biogeochemical float deployment strategy, with example from the Greenwich Meridian line (GO-SHIP A12). *J. Geophys. Res. Oceans* **124**, 403–431 (2019).
10. S. M. Bushinsky, P. Landschützer, C. Rödenbeck, A. R. Gray, D. Baker, M. R. Mazloff, L. Resplandy, K. S. Johnson, J. L. Sarmiento, Reassessing Southern Ocean air-sea CO_2 flux estimates with the addition of biogeochemical float observations. *Global Biogeochem. Cycles* **33**, 1370–1388 (2019).
11. A. R. Gray, K. S. Johnson, S. M. Bushinsky, S. C. Riser, J. L. Russell, L. D. Talley, R. Wanninkhof, N. L. Williams, J. L. Sarmiento, Autonomous biogeochemical floats detect significant carbon dioxide outgassing in the high-latitude Southern Ocean. *Geophys. Res. Lett.* **45**, 9049–9057 (2018).
12. P. Friedlingstein, M. O'Sullivan, M. W. Jones, R. M. Andrew, L. Gregor, J. Hauck, C. Le Quéré, I. T. Luijkx, A. Olsen, G. P. Peters, W. Peters, J. Pongratz, C. Schwingshackl, S. Sitch, J. G. Canadell, P. Ciais, R. B. Jackson, S. R. Alin, R. Alkama, A. Arneth, V. K. Arora, N. R. Bates, M. Becker, N. Bellouin, H. C. Bittig, L. Bopp, F. Chevallier, L. P. Chini, M. Cronin, W. Evans, S. Falk, R. A. Feely, T. Gasser, M. Gehlen, T. Gkritzalis, L. Gloege, G. Grassi, N. Gruber, Ö. Gürses, I. Harris, M. Hefner, R. A. Houghton, G. C. Hurtt, Y. Iida, T. Ilyina, A. K. Jain, A. Jersild, K. Kadono, E. Kato, D. Kennedy, K. Klein Goldewijk, J. Knauer, J. I. Korsbakken, P. Landschützer, N. Lefèvre, K. Lindsay, J. Liu, Z. Liu, G. Marland, N. Mayot, M. J. McGrath, N. Metzl, N. M. Monacci, D. R. Munro, S.-I. Nakaoka, Y. Niwa, K. O'Brien, T. Ono, P. I. Palmer, N. Pan, D. Pierrot, K. Pocock, B. Poulter, L. Resplandy, E. Robertson, C. Rödenbeck, C. Rodriguez, T. M. Rosan, J. Schwinger, R. Séférian, J. D. Shutler, I. Skjelvan, T. Steinhoff, Q. Sun, A. J. Sutton, C. Sweeney, S. Takao, T. Tanhua, P. P. Tans, X. Tian, H. Tian, B. Tilbrook, H. Tsujino, F. Tubiello, G. R. van der Werf, A. P. Walker, R. Wanninkhof, C. Whitehead, A. Willstrand Wranne, R. Wright, W. Yuan, C. Yue, X. Yue, S. Zaehle, J. Zeng, B. Zheng, Global carbon budget 2022. *Earth Syst. Sci. Data* **14**, 4811–4900 (2022).
13. Y. Dong, D. C. E. Bakker, T. G. Bell, B. Huang, P. Landschützer, P. S. Liss, M. Yang, Update on the temperature corrections of global air-sea CO_2 flux estimates. *Global Biogeochem. Cycles* **36**, e2022GB007360 (2022).
14. A. J. Watson, U. Schuster, J. D. Shutler, T. Holding, I. G. C. Ashton, P. Landschützer, D. K. Woolf, L. Goddijn-Murphy, Revised estimates of ocean-atmosphere CO_2 flux are consistent with ocean carbon inventory. *Nat. Commun.* **11**, 1–6 (2020).
15. L. P. M. S. Monteiro, L. Gregor, M. Lévy, S. Maenner, C. L. Sabine, S. Swart, Intraseasonal variability linked to sampling alias in air-sea CO_2 fluxes in the Southern Ocean. *Geophys. Res. Lett.* **42**, 8507–8514 (2015).
16. A. J. Sutton, N. L. Williams, B. Tilbrook, Constraining Southern Ocean CO_2 flux uncertainty using Uncrewed Surface Vehicle observations. *Geophys. Res. Lett.* **48**, 1–9 (2021).
17. L. M. Djeutchouang, N. Chang, L. Gregor, M. Vichi, P. M. S. Monteiro, The sensitivity of pCO_2 reconstructions to sampling scales across a Southern Ocean sub-domain: A semi-idealized ocean sampling simulation approach. *Biogeosciences* **19**, 4171–4195 (2022).
18. S. A. Nicholson, D. B. Whitt, I. Fer, M. D. du Plessis, A. D. Lebéhot, S. Swart, A. J. Sutton, P. M. S. Monteiro, Storms drive outgassing of CO_2 in the subpolar Southern Ocean. *Nat. Commun.* **13**, 1–12 (2022).
19. R. Wanninkhof, Relationship between wind speed and gas exchange over the ocean revisited. *Limnol. Oceanogr. Methods* **12**, 351–362 (2014).
20. D. K. Woolf, J. D. Shutler, L. Goddijn-Murphy, A. J. Watson, B. Chapron, P. D. Nightingale, C. J. Donlon, J. Piskozub, M. J. Yelland, I. Ashton, T. Holding, U. Schuster, F. Girard-Ardhuin, A. Grouazel, J. F. Piolle, M. Warren, I. Wrobel-Niedzwiecka, P. E. Land, R. Torres, J. Prytherch, B. Moat, J. Hanafin, F. Ardhuin, F. Paul, Key uncertainties in the recent air-sea flux of CO_2. *Global Biogeochem. Cycles* **33**, 1548–1563 (2019).
21. M. Yang, T. G. Bell, J. R. Bidlot, B. W. Blomquist, B. J. Butterworth, Y. Dong, C. W. Fairall, S. Landwehr, C. A. Marandino, S. D. Miller, E. S. Saltzman, A. Zavarsky, Global synthesis of air-sea CO_2 transfer velocity estimates from ship-based eddy covariance measurements. *Front. Mar. Sci.* **9**, 1–15 (2022).
22. Y. Dong, M. Yang, D. C. E. Bakker, V. Kitidis, T. G. Bell, Uncertainties in eddy covariance air-sea CO_2 flux measurements and implications for gas transfer velocity parameterisations. *Atmos. Chem. Phys.* **21**, 8089–8110 (2021).
23. P. Friedlingstein, M. W. Jones, M. O'Sullivan, R. M. Andrew, D. C. E. Bakker, J. Hauck, C. Le Quéré, G. P. Peters, W. Peters, J. Pongratz, S. Sitch, J. G. Canadell, P. Ciais, R. B. Jackson, S. R. Alin, P. Anthoni, N. R. Bates, M. Becker, N. Bellouin, L. Bopp, T. T. T. Chau, F. Chevallier, L. P. Chini, M. Cronin, K. I. Currie, B. Decharme, L. M. Djeutchouang, X. Dou, W. Evans, R. A. Feely, L. Feng, T. Gasser, D. Gilfillan, T. Gkritzalis, G. Grassi, L. Gregor, N. Gruber, Ö. Gürses, I. Harris, R. A. Houghton, G. C. Hurtt, Y. Iida, T. Ilyina, I. T. Luijkx, A. Jain, S. D. Jones, E. Kato, D. Kennedy, K. Klein Goldewijk, J. Knauer, J. I. Korsbakken, A. Körtzinger, P. Landschützer, S. K. Lauvset, N. Lefèvre, S. Lienert, J. Liu, G. Marland, P. C. McGuire, J. R. Melton, D. R. Munro, J. E. M. S. Nabel, S.-I. Nakaoka, Y. Niwa, T. Ono, D. Pierrot, B. Poulter, G. Rehder, L. Resplandy, E. Robertson, C. Rödenbeck, T. M. Rosan, J. Schwinger, C. Schwingshackl, R. Séférian, A. J. Sutton, C. Sweeney, T. Tanhua, P. P. Tans, H. Tian, B. Tilbrook, F. Tubiello, G. R. van der Werf, N. Vuichard, C. Wada, R. Wanninkhof, A. J. Watson, D. Willis, A. J. Wiltshire, W. Yuan, C. Yue, X. Yue, S. Zaehle, J. Zeng, Global carbon budget 2021. *Earth Syst. Sci. Data* **14**, 1917–2005 (2022).
24. J. Hauck, M. Zeising, C. Le Quéré, N. Gruber, D. C. E. Bakker, L. Bopp, T. T. T. Chau, Ö. Gürses, T. Ilyina, P. Landschützer, A. Lenton, L. Resplandy, C. Rödenbeck, J. Schwinger, R. Séférian, Consistency and challenges in the ocean carbon sink estimate for the global carbon budget. *Front. Mar. Sci.* **7**, 1–22 (2020).
25. Y. Park, T. Park, T. Kim, S. Lee, C. Hong, J. Lee, M. Rio, M. Pujol, M. Ballarotta, I. Durand, Observations of the Antarctic Circumpolar Current over the Udintsev Fracture Zone, the narrowest choke point in the Southern Ocean. *J. Geophys. Res. Oceans* **124**, 4511–4528 (2019).
26. C. Rödenbeck, D. C. E. Bakker, N. Metzl, A. Olsen, C. Sabine, N. Cassar, F. Reum, R. F. Keeling, M. Heimann, Interannual sea-air CO_2 flux variability from an observation-driven ocean mixed-layer scheme. *Biogeosciences* **11**, 4599–4613 (2014).
27. A. R. Fay, L. Gregor, P. Landschützer, G. A. McKinley, N. Gruber, M. Gehlen, Y. Iida, G. G. Laruelle, C. Rödenbeck, A. Roobaert, J. Zeng, SeaFlux: Harmonization of air-sea CO_2 fluxes from surface pCO_2 data products using a standardized approach. *Earth Syst. Sci. Data* **13**, 4693–4710 (2021).
28. T. Naegler, Reconciliation of excess ^{14}C-constrained global CO_2 piston velocity estimates. *Tellus B Chem. Phys. Meteorol.* **61B**, 372–384 (2009).
29. M. C. Long, B. B. Stephens, K. McKain, C. Sweeney, R. F. Keeling, E. A. Kort, E. J. Morgan, J. D. Bent, N. Chandra, F. Chevallier, Strong Southern Ocean carbon uptake evident in airborne observations. *Science* **374**, 1275–1280 (2021).
30. P. Regnier, L. Resplandy, R. G. Najjar, P. Ciais, The land-to-ocean loops of the global carbon cycle. *Nature* **603**, 401–410 (2022).
31. J. D. Müller, N. Gruber, B. R. Carter, R. A. Feely, M. Ishii, N. Lange, S. K. Lauvset, A. M. Murata, A. Olsen, F. F. Pérez, C. L. Sabine, T. Tanhua, R. Wanninkhof, D. Zhu, Decadal trends in the oceanic storage of anthropogenic carbon from 1994 to 2014. *AGU Adv.* **4**, e2023AV000875 (2023).

32. N. L. Williams, L. W. Juranek, R. A. Feely, K. S. Johnson, J. L. Sarmiento, L. D. Talley, A. G. Dickson, A. R. Gray, R. Wanninkhof, J. L. Russell, S. C. Riser, Y. Takeshita, Calculating surface ocean pCO_2 from biogeochemical Argo floats equipped with pH: An uncertainty analysis. *Global Biogeochem. Cycles* **31**, 591–604 (2017).
33. S. M. Bushinsky, I. Cerovečki, Subantarctic mode water biogeochemical formation properties and interannual variability. *AGU Adv.* **4**, e2022AV000722 (2023).
34. N. Mackay, A. Watson, J., Winter air-sea CO_2 fluxes constructed from summer observations of the polar southern ocean suggest weak outgassing. *Geophys. Res. Ocean.* **126**, e2020JC016600 (2021).
35. Y. Wu, D. C. E. Bakker, E. P. Achterberg, A. N. Silva, D. D. Pickup, X. Li, S. Hartman, D. Stappard, D. Qi, T. Tyrrell, Integrated analysis of carbon dioxide and oxygen concentrations as a quality control of ocean float data. *Commun. Earth Environ.* **3**, 92 (2022).
36. D. C. E. Bakker, S. R. Alin, N. Bates, M. Becker, R. A. Feely, T. Gkritzalis, S. D. Jones, A. Kozyr, S. K. Lauvset, N. Metzl, D. R. Munro, S. Nakaoka, Y. Nojiri, K. M. O'Brien, A. Olsen, D. Pierrot, G. Rehder, T. Steinhoff, A. J. Sutton, C. Sweeney, B. Tilbrook, C. Wada, R. Wanninkhof, J. Akl, L. Barbero, C. M. Beatty, C. F. Berghoff, H.C. Bittig, R. Bott, E. F. Burger, W. Cai, R. Castaño-Primo, J. E. Corredor, M. Cronin, E. H. De Carlo, M. D. DeGrandpre, C. Dietrich, W. M. Drennan, S. R. Emerson, I. C. Enochs, K. Enyo, L. Epherra, W. Evans, B. Fiedler, M. Fontela, C. Frangoulis, M. Gehrung, L. Giannoudi, M. Glockzin, B. Hales, S. D. Howden, J. S.P. Ibánhez, L. Kamb, A. Körtzinger, N. Lefèvre, C. Lo Monaco, V. A. Lutz, V. A. Macovei, S. Maenner Jones, D. Manalang, D. P. Manzello, N. Metzl, J. Mickett, F. J. Millero, N. M. Monacci, J. M. Morell, S. Musielewicz, C. Neill, T. Newberger, J. Newton, S. Noakes, S. R. Ólafsdóttir, T. Ono, J. Osborne, X. A. Padín, M. Paulsen, L. Perivoliotis, W. Petersen, G. Petihakis, A. J. Plueddemann, C. Rodriguez, A. Rutgersson, C. L. Sabine, J. E. Salisbury, R. Schlitzer, I. Skjelvan, N. Stamataki, K. F. Sullivan, S. C. Sutherland, M. T'Jampens, K. Tadokoro, T. Tanhua, M. Telszewski, H. Theetaert, M. Tomlinson, D. Vandemark, A. Velo, Y. G. Voynova, R. A. Weller, C. Whitehead, C. Wimart-Rousseau, Surface Ocean CO2 Atlas Database Version 2023 (SOCATv2023) (NCEI Accession 0278913). NOAA National Centers for Environmental Information Dataset. https://doi.org/10.25921/r7xa-bt92.
37. R. Wanninkhof, W. E. Asher, D. T. Ho, C. Sweeney, W. R. McGillis, Advances in quantifying air-sea gas exchange and environmental forcing. *Annu. Rev. Mar. Sci.* **1**, 213–244 (2009).
38. R. F. Weiss, Carbon dioxide in water and seawater: The solubility of a non-ideal gas. *Mar. Chem.* **2**, 203–215 (1974).
39. D. K. Woolf, P. E. Land, J. D. Shutler, L. M. Goddijn-Murphy, C. J. Donlon, On the calculation of air-sea fluxes of CO_2 in the presence of temperature and salinity gradients. *J. Geophys. Res. Oceans* **121**, 1229–1248 (2016).
40. T. T. T. Chau, M. Gehlen, F. Chevallier, A seamless ensemble-based reconstruction of surface ocean pCO_2 and air-sea CO_2 fluxes over the global coastal and open oceans. *Biogeosciences* **19**, 1087–1109 (2022).
41. L. Gregor, N. Gruber, OceanSODA-ETHZ: A global gridded data set of the surface ocean carbonate system for seasonal to decadal studies of ocean acidification. *Earth Syst. Sci. Data* **13**, 777–808 (2021).
42. L. Gregor, A. D. Lebehot, S. Kok, P. M. S. Monteiro, A comparative assessment of the uncertainties of global surface ocean CO_2 estimates using a machine-learning ensemble (CSIR-ML6 version 2019a) – have we hit the wall? *Geosci. Model Dev.* **12**, 5113–5136 (2019).
43. Y. Iida, Y. Takatani, A. Kojima, M. Ishii, Global trends of ocean CO_2 sink and ocean acidification: An observation-based reconstruction of surface ocean inorganic carbon variables. *J. Oceanogr.* **77**, 323–358 (2021).
44. P. Landschützer, N. Gruber, D. C. E. Bakker, Decadal variations and trends of the global ocean carbon sink. *Global Biogeochem. Cycles* **30**, 1396–1417 (2016).
45. J. Zeng, Y. Nojiri, P. Landschützer, M. Telszewski, S. Nakaoka, A global surface ocean fCO_2 climatology based on a feed-forward neural network. *J. Atmos. Ocean. Technol.* **31**, 1838–1849 (2014).
46. H. Hersbach, B. Bell, P. Berrisford, S. Hirahara, A. Horányi, J. Muñoz-Sabater, J. Nicolas, C. Peubey, R. Radu, D. Schepers, A. Simmons, C. Soci, S. Abdalla, X. Abellan, G. Balsamo, P. Bechtold, G. Biavati, J. Bidlot, M. Bonavita, G. De Chiara, P. Dahlgren, D. Dee, M. Diamantakis, R. Dragani, J. Flemming, R. Forbes, M. Fuentes, A. Geer, L. Haimberger, S. Healy, R. J. Hogan, E. Hólm, M. Janisková, S. Keeley, P. Laloyaux, P. Lopez, C. Lupu, G. Radnoti, P. de Rosnay, I. Rozum, F. Vamborg, S. Villaume, J. N. Thépaut, The ERA5 global reanalysis. *Q. J. R. Meteorol. Soc.* **146**, 1999–2049 (2020).
47. R. W. Reynolds, T. M. Smith, C. Liu, D. B. Chelton, K. S. Casey, M. G. Schlax, Daily high-resolution-blended analyses for sea surface temperature. *J. Climate* **20**, 5473–5496 (2007).
48. C. W. Fairall, E. F. Bradley, J. S. Godfrey, G. A. Wick, J. B. Edson, G. S. Young, Cool-skin and warm-layer effects on sea surface temperature. *J. Geophys. Res. Oceans* **101**, 1295–1308 (1996).
49. F. Xu, A. Ignatov, In situ SST quality monitor (i Quam). *J. Atmos. Ocean. Technol.* **31**, 164–180 (2014).
50. F. Lacroix, T. Ilyina, J. Hartmann, Oceanic CO_2 outgassing and biological production hotspots induced by pre-industrial river loads of nutrients and carbon in a global modeling approach. *Biogeosciences* **17**, 55–88 (2020).
51. V. Kitidis, I. Brown, N. Hardman-Mountford, N. Lefèvre, Surface ocean carbon dioxide during the Atlantic Meridional Transect (1995–2013); evidence of ocean acidification. *Prog. Oceanogr.* **158**, 65–75 (2017).
52. M. Yang, T. J. Smyth, V. Kitidis, I. J. Brown, C. Wohl, M. J. Yelland, T. G. Bell, Natural variability in air-sea gas transfer efficiency of CO_2. *Sci. Rep.* **11**, 1–9 (2021).
53. J. B. Edson, A. A. Hinton, K. E. Prada, J. E. Hare, C. W. Fairall, Direct covariance flux estimates from mobile platforms at sea. *J. Atmos. Ocean. Technol.* **15**, 547–562 (1998).
54. B. W. Blomquist, S. E. Brumer, C. W. Fairall, B. J. Huebert, C. J. Zappa, I. M. Brooks, M. Yang, L. Bariteau, J. Prytherch, J. E. Hare, H. Czerski, A. Matei, R. W. Pascal, Wind speed and sea state dependencies of air-sea gas transfer: Results from the High Wind Speed Gas Exchange Study (HiWinGS). *J. Geophys. Res. Oceans* **122**, 8034–8062 (2017).
55. S. Landwehr, S. D. Miller, M. J. Smith, E. S. Saltzman, B. Ward, Analysis of the PKT correction for direct CO_2 flux measurements over the ocean. *Atmos. Chem. Phys.* **14**, 3361–3372 (2014).
56. S. D. Miller, C. Marandino, E. S. Saltzman, Ship-based measurement of air-sea CO_2 exchange by eddy covariance. *J. Geophys. Res. Atmos.* **115**, 1–14 (2010).
57. E. Nilsson, H. Bergström, A. Rutgersson, E. Podgrajsek, M. B. Wallin, G. Bergström, E. Dellwik, S. Landwehr, B. Ward, Evaluating humidity and sea salt disturbances on CO_2 flux measurements. *J. Atmos. Ocean. Technol.* **35**, 859–875 (2018).
58. D. T. Ho, C. S. Law, M. J. Smith, P. Schlosser, M. Harvey, P. Hill, Measurements of air-sea gas exchange at high wind speeds in the Southern Ocean: Implications for global parameterizations. *Geophys. Res. Lett.* **33**, L16611 (2006).
59. T. G. Bell, S. Landwehr, S. D. Miller, W. J. De Bruyn, A. H. Callaghan, B. Scanlon, B. Ward, M. Yang, E. S. Saltzman, Estimation of bubble-mediated air-sea gas exchange from concurrent DMS and CO_2 transfer velocities at intermediate-high wind speeds. *Atmos. Chem. Phys.* **17**, 9019–9033 (2017).
60. R. Pereira, I. Ashton, B. Sabbaghzadeh, J. D. Shutler, R. C. Upstill-Goddard, Reduced air-sea CO_2 exchange in the Atlantic Ocean due to biological surfactants. *Nat. Geosci.* **11**, 492–496 (2018).
61. C. W. Fairall, M. Yang, S. E. Brumer, B. W. Blomquist, J. B. Edson, C. J. Zappa, L. Bariteau, S. Pezoa, T. G. Bell, E. S. Saltzman, Air-sea trace gas fluxes: Direct and indirect measurements. *Front. Mar. Sci.* **9**, 1–16 (2022).
62. I. R. Young, E. Fontaine, Q. Liu, A. V. Babanin, The wave climate of the Southern Ocean. *J. Phys. Oceanogr.* **50**, 1417–1433 (2020).
63. S. Kobayashi, Y. Ota, Y. Harada, A. Ebita, M. Moriya, H. Onoda, K. Onogi, H. Kamahori, C. Kobayashi, H. Endo, The JRA-55 reanalysis: General specifications and basic characteristics. *J. Meteorol. Soc. Jpn. Ser.* **93**, 5–48 (2015).
64. S. C. Doney, I. Lima, R. A. Feely, D. M. Glover, K. Lindsay, N. Mahowald, J. K. Moore, R. Wanninkhof, Mechanisms governing interannual variability in upper-ocean inorganic carbon system and air-sea CO_2 fluxes: Physical climate and atmospheric dust. *Deep Sea Res. Part II Top. Stud. Oceanogr.* **56**, 640–655 (2009).
65. S. Berthet, R. Séférian, C. Bricaud, M. Chevallier, A. Voldoire, C. Ethé, Evaluation of an online grid-coarsening algorithm in a global Eddy-Admitting ocean biogeochemical model. *J. Adv. Model. Earth Syst.* **11**, 1759–1783 (2019).
66. O. Aumont, C. Ethé, A. Tagliabue, L. Bopp, M. Gehlen, PISCES-v2: An ocean biogeochemical model for carbon and ecosystem studies. *Geosci. Model Dev.* **8**, 2465–2513 (2015).
67. E. T. Buitenhuis, T. Hashioka, C. Le Quéré, Combined constraints on global ocean primary production using observations and models. *Global Biogeochem. Cycles* **27**, 847–858 (2013).
68. J. Schwinger, N. Goris, J. F. Tjiputra, I. Kriest, M. Bentsen, I. Bethke, M. Ilicak, K. M. Assmann, C. Heinze, Evaluation of NorESM-OC (versions 1 and 1.2), the ocean carbon-cycle stand-alone configuration of the Norwegian Earth System Model (NorESM1). *Geosci. Model Dev.* **9**, 2589–2622 (2016).
69. A. Adcroft, W. Anderson, V. Balaji, C. Blanton, M. Bushuk, C. O. Dufour, J. P. Dunne, S. M. Griffies, R. Hallberg, M. J. Harrison, The GFDL global ocean and sea ice model OM4. 0: Model description and simulation features. *J. Adv. Model. Earth Syst.* **11**, 3167–3211 (2019).
70. H. Paulsen, T. Ilyina, K. D. Six, I. Stemmler, Incorporating a prognostic representation of marine nitrogen fixers into the global ocean biogeochemical model HAMOCC. *J. Adv. Model. Earth Syst.* **9**, 438–464 (2017).

Acknowledgments: We are grateful to M. García-Ibáñez (Institute de Ciències del Mar) for helping subsample the flux product and to P. Suntharalingam (University of East Anglia), A. Rutgersson (Uppsala University), L. Bopp (Institute Pierre-Simon Laplace), and Y. Tham (Sun Yat-Sen University) for in-depth discussions. We would also thank the captains and crew of RRS *James Clark Ross* and RRS *Discovery* and all those who helped keep the CO_2 flux system running. The Surface Ocean CO_2 Atlas (SOCAT) is an international effort, endorsed by the International Ocean Carbon Coordination Project (IOCCP), the Surface Ocean Lower Atmosphere Study (SOLAS), and the Integrated Marine Biogeochemistry and Ecosystem Research program (IMBER), to deliver a uniformly quality-controlled surface ocean CO_2 database. D. Bakker chairs the SOCAT global group, and the many researchers and funding

agencies responsible for the collection of data and quality control are thanked for their contributions to SOCAT. **Funding:** Y.D. has been supported by the China Scholarship Council (CSC/201906330072). The Natural Environment Research Council (NERC) has enabled D.C.E.B.'s work (PICCOLO, NE/P021395/1, and CUSTARD, NE/P021263/1 projects). The contributions of T.G.B. and M.Y. have been made possible by support from NERC (ORCHESTRA, NE/N018095/1, and PICCOLO NE/P021409/1 projects) and the European Space Agency AMT4oceanSatFluxCCN (4000125730/18/NL/FF/gp). Funding to J.H. was provided by the Initiative and Networking Fund of the Helmholtz Association [Helmholtz Young Investigator Group Marine Carbon and Ecosystem Feedbacks in the Earth System (MarESys), grant VH-NG-1301], by the ERC-2022-STG OceanPeak (grant 101077209), and by the European Union's Horizon Europe research and innovation program under grant 101083922 (OceanICU Improving Carbon Understanding). The work reflects only the authors' view; the European Commission and their executive agency are not responsible for any use that may be made. **Author contributions:** Y.D., T.G.B., M.Y. D.C.E.B., P.L., J.H., and C.R. conceived this study. Y.D. performed the data analysis and produced the figures. All authors contributed ideas and discussed the results. D.C.E.B., P.S.L., T.G.B., and M.Y. provided supervision. Y.D. wrote the initial draft, and all coauthors contributed to the writing. **Competing interests:** The authors declare that they have no competing interests. **Data and materials availability:** All data needed to evaluate the conclusions in the paper are present in the paper and/or the Supplementary Materials. The MPI-SOMFFN product and the cruise data including the EC flux observations and subsampled flux products: http://doi.org/10.5061/dryad.b2rbnzspm. The CarboScope product: https://www.bgc-jena.mpg.de/CarboScope/?ID=oc_v2021 (SOCAT-based product); https://www.bgc-jena.mpg.de/CarboScope/?ID=oc_SOCCOM_v2021 (SOCAT plus SOCCOM–based product); https://www.bgc-jena.mpg.de/CarboScope/?ID=oc_SOCCOMonly_v2022 (SOCCOM-weighted product). The SOCAT fCO_2 measurements v2021: https://socat.info/index.php/version-2021/. The derived SOCCOM fCO_2 data (2015–2020): http://doi.org/10.6075/J0BK19W5.

Submitted 17 December 2023
Accepted 18 June 2024
Published 24 July 2024
10.1126/sciadv.adn5781